PAPER

Check for updates

Surface refined Au^{Quercetin} nanoconjugate stimulates dermal cell migration: possible implication in wound healing†

Madhyastha H., [iD] ‡*[a] Halder S.,[b] Queen Intan N.,[a] Madhyastha R.,[a] Mohanapriya A.,[b] Sudhakaran R.,[b] Sajitha L. S.,[b] Banerjee K.,[b] Bethasiwi P., [iD] [a] Daima H.,[c] Navya P. N.,[d] Maruyama M.[a] and Nakajima Y. [iD] ‡*[a]

Refining nutraceutical conjugated metal nanoparticles (NPs) and understanding their interactions with the cellular micro-environment is necessary for their application in nanomedicine. In the present experiment, we studied the effect of quercetin functionalized gold nanoparticles (Au^{Qur}NP) on skin fibroblast and keratinocyte cell migration. Spherical shaped Au^{Qur}NPs of 47 nm in size were formed due to the interaction of hydroxyl and carbonyl groups of quercetin with Au atoms as revealed by incremental algorithm-based analysis. Au^{Qur}NP containing up to 5 μg l^{-1} of Au with quercetin (5.2 ± 1.6 ng ml^{-1}) was least toxic to fibroblasts. Au^{Qur}NP effectively reduced the generation of intracellular ROS (up to 63%) through free-radical scavenging activity. Au^{Qur}NP also enhanced the rate of migration of fibroblasts (24 h) and keratinocytes (20 h) in artificially created wounds. The rate of migration of the cells towards the wound edge was in the order of Au^{Qur}NP > control > quercetin > AuNP. Au^{Qur}NP also significantly increased the expression of TGFβ1 protein, thereby inducing the downstream SMAD complex (SMAD 2–4). Downregulation of the inhibitory protein SMAD 7 by Au^{Qur}NP helped in the nuclear translocation of SMADs 3 and 4. Collectively, the present *in vitro* study demonstrates the action of Au^{Qur}NP on the SMAD family and the interconnected molecular mechanism leading to the cell migration process.

Introduction

Nanotechnology, encompassing the utilization of physical, chemical and biological systems at submicron levels, opens the flood gate of information for new drug design and application. Advances in nanomaterials and their application in biological modules is considered as cutting-edge research and is advancing rapidly in the field of nanotechnology.[1] Nano-materials have a wide range of applications such as in drug synthesis, environmental science, regenerative medicine, food technology, and vaccine development, due to their unique nanoscale size, increased surface area, and high mechanical strength and potential electronic, magnetic and photonic properties. Nanomaterial assisted drug delivery is becoming an advanced tool in regenerative medicine as it over overcomes the limitation of conventional drug delivery system. Sources of drug synthesis are either synthetic chemistry based or from natural sources.[2] Bio-inspired smart hybridization with natural compounds is gaining considerable attention as a green route to nanoparticle synthesis, and is emerging as an important and sustainable eco-friendly approach for nano-formulations. Drug designers are increasingly interested in developing multi-targeted therapy strategies by conjugation reaction with biocompatible metals. Over the last decade, research has expanded on widely used metals like gold, silver, copper, iron, and zinc as sources for nanomaterial synthesis.[3] Among all metals, gold and silver nanoparticles (NPs) have huge potentials as drug carriers and anti-bacterial agents in regenerative medicine.[4]

Quercetin, a bioflavonoid commonly found in fruits, vege-tables, seeds, berries, and tea, has been studied extensively for prevention of osteoporosis, cardiovascular disease, tumors, allergy, inflammation, and cancer.[5,6] Despite promising bio-efficacy credits of quercetin, a major drawback limiting its clinical efficacy is its poor bio-availability due to low solubility in aqueous solution. Rapid hydrolysis due to extreme gastric pH condition in gastrointestinal tract is another bottle neck that decreases its bioactivity index. Recently various attempts, such

[a]*Department of Applied Physiology, Faculty of Medicine, University of Miyazaki, Miyazaki 889 1692, Japan. E-mail: hkumar@med.miyazaki-u.ac.jp; Yunakaji@med.miyazaki-u.ac.jp*

[b]*School of Biosciences and Technology, Vellore Institute of Technology, Vellore 632014, Tamilnadu, India*

[c]*Amity Center for Nanobiotechnology and Nanomedicine, Amity Institute of Biotechnology, Amity University Rajasthan, Jaipur 303002, Rajasthan, India*

[d]*Department of Biotechnology, Bannari Amman Institute of Technology, Sathyamangalam, Erode 638401, Tamilnadu, India*

† Electronic supplementary information (ESI) available. See DOI: 10.1039/d0ra06690g

‡ Equal contribution.

as incorporating it into NPs,[7–13] apoferritin loaded system,[14] and hydrogel formulation[15,16] have been made to increase its biopotencies.

In spite of vast knowledge on quercetin and its application in management of various regenerative diseases, some inherent short-comings still persists in dermal wound healing complications. Skin abnormalities suffers both from internal as well as external stimuli. Common dermatologic ailments include skin atopy, psoriasis, keratosis, skin cancer, autoimmune bullous skin diseases, acne vulgaris, chronic non-healing wounds, skin pigmentation disorder *etc.*[17] Chronic non-healing wound is a major source of concern for pathologists and dermatological clinicians. Wound and its healing process is a dynamic process involving inflammation, proliferation and remodeling phases, each employing several cascades of biochemical pathways and interconnected signal transduction cross talk.[18–21] In recent years, nanotechnology directed technologies are gaining recognition as therapeutic agents in wound healing scenario.[22,23] However, their clinical applications have several limitations due to drug instability, drug precipitations, toxicity, and skin permeation.

We had previously synthesized quercetin conjugated gold nanoparticles (Au^Qur^NP) and showed its beneficial effects on skin fibroblasts.[24] The current investigation aims to validate the effect of Au^Qur^NP on the process of migration of fibroblasts in artificially created *in vitro* wound model and understand the associated molecular mechanism. We demonstrate that Au^Qur^NP enhances fibroblast migration through TGFβ1 mediated SMAD signaling cascade.

Materials and methods

Chemicals and reagents

Tetrachloroaouric acid (AuCl₄), quercetin, potassium hydroxide (KOH), Tween-20, DMSO, MTT [3-(4,5-dimethylthiazol-2-yl)-2-5-diphenyltetrazolium bromide], *N*-acetyl cysteine (*NAC*), crystal violet, Stemline Keratinocyte medium II (#S0196) were purchased from Sigma-Aldrich (St., Louis, MO, USA). Mouse skin fibroblast cell line m5S and human keratinocyte cell line PHK16-0b were purchased from National Institute of Biomedical Innovation, Health and Nutrition cell bank (NIBIHON, Ibaraki, Japan). Cell culture medium (α MEM), antibacterial cocktail (PSN), and FBS were procured from Nacalai Tesque (Tokyo, Japan). Primary antibodies for TGFβ1, SMAD 2–4, 7, and β-actin, and respective secondary antibodies were purchased from Cell Signaling technologies (MA, USA). Au^Qur^NP synthesis and characterization was performed as per previously adopted method.[24]

Molecular docking and bioinformatics analysis

Interaction of quercetin with Au atom was predicted by Flex X systems to predict the interaction of specific protein ligands with specific moiety on the basis of discrete model.[25] The Au docking results were validated with re-docking the ligands with proteins sites of quercetin and comparing the Root Mean Square Deviation (RMSD).

Characterization of Au^Qur^NP

We previously reported the synthesis, physico-chemical and instrumental characterization of Au^Qur^NP.[24] Suspensions of colloidal samples were air dried and loaded on copper grids at room temperature. The samples were then processed by transmission electron microscopy (TEM) under high vacuum as per standard methods (HT 7700, Hitachi-High technologies Corporation, Tokyo, Japan). The working condition of instruments included voltage of 800 kV and magnification at 125k times. The standard scale bar according to magnification is default programed by manufacturer (scale bar to 125k magnification is 100 nm). Au^Qur^NPs were denatured by surface bleaching method to get AuNPs.

Cytotoxicity and cell proliferation assay

4×10^4 cells per ml m5S fibroblasts (third passage) were cultured in α MEM conditioned with 10% FBS and 1% antibacterial cocktail at 37 °C, 5% CO_2 and 95% humidity. Fibroblasts were treated with different doses of AuNP or Au^Qur^NP (0, 0.5, 1.0, 5.0 and 10.0 µg l⁻¹) for 16 h. Percentage of viable cells were analyzed by MTT assay.[26] Same procedure was employed for time dependent cytotoxicity and cell viability studies, after treatment with 5 µg l⁻¹ AuNP or Au^Qur^NP at different time interval (0, 2, 4, 8, 16 and 24 h). Intracellular purple formazan was quantified with spectrophotometer at absorbance of 570 nm (Multiskan FC, Thermo Fisher Scientific Inc., Pittsburg, PA, USA).

Intracellular ROS production assay

m5S cells treated with 5 µg l⁻¹ AuNPs or Au^Qur^NPs for 8 h, were analyzed for intracellular ROS production. Untreated cells were used as control group. Oxyselect ROS detection kit was used to evaluate the ROS production as per manufacturer's instructions (Cell Biolabs. Inc. San Diego, USA). Fluorescence intensity of ROS production was obtained by using fluorescence microscope (TCS SP8, Leica, Wetzler, Germany).

DPPH radical scavenging assay

Free-radical scavenging efficiency of the NPs were analyzed by DPPH reduction method. Different doses of AuNP or Au^Qur^NP (0, 0.5, 1.0, 5.0 and 10.0 µg l⁻¹) were mixed with DPPH solution and absorbance was measured at 570 nm (Multiskan FC, Thermo Fisher Scientific Inc., Pittsburg, PA, USA). Change in color of DPPH from violet to yellow was used as an index of free-radical scavenging efficacy of the NPs. Results are presented as mean value of nine determinations. Percentage of radical scavenging was calculated by using the following formula.

$$\text{Radical scavenging}\% = 100 \frac{A_{\text{control}} - A_{\text{sample}}}{A_{\text{control}}}$$

A_{control}: the absorbance of control DPPH solution; A_{sample}: absorbance of the sample Au^Qur^NPs mixed with DPPH solution.

Cell morphometry assay

m5S cells cultured on culture-suitable cover slips were treated with 5 µg l^{-1} AuNP or Au^{Qur}NP for 8 h. After treatment, cells were fixed with 4% PFA for 10 min at room temperature. Fixed cells were treated with cell permeable crystal violet dye for 5 min, washed several times with MilliQ water to remove excess dye, dried at room temperature, and photographed using bright field microscope (BX-43, Olympus Co. Ltd., Tokyo, Japan).

Quercetin entrapment assay

Au^{Qur}NP was suspended in MilliQ water and sonicated (500 Hz s^{-1}) at 37 °C in water bath for 5 min (Power Sonic, Co., Ltd, Hwashion technology, Seoul, Korea). Supernatant was collected and the released quercetin was measured by spectrophotometer (Shimadzu UV/Vis spectrophotometer, Tokyo, Japan) at wavelength of 372 nm. All measurements were repeated in triplicates and data expressed as mean ± standard deviation. Quercetin encapsulation efficiency was calculated according to standard formula of regression analysis by using standard quercetin.

$$\% \text{ encapsulation efficiency} = [(\text{total amount of quercetin added} - \\ \text{amount of free quercetin in supernatant}/ \\ \text{total amount of quercetin added})] \times 100.$$

RT-PCR analysis

m5S cells (4×10^4 cells per ml) were cultured in 6 well culture dish and incubated with various doses of Au^{Qur}NP (0, 0.5, 1.0, 5.0 and 10 µg l^{-1}) or pure quercetin (2 ng ml^{-1}) for 4 h. Treated cells were washed with cold PBS and total RNA was isolated using RNAiso (Takara, Tokyo, Japan) as per manufacturer's protocol. One µg RNA was used to synthesize first strand cDNA using ReverTra Ace enzyme (Toyobo, Tokyo, Japan) and processed for PCR reaction using GoTaq Green master mix (Promega, USA) for analysis of TGFβ1 (forward 5′-CTGTCCAAACTAAGGCTCGC-3′; reverse 5′-CGTCAAAAGACAGCCACTCA-3′) gene expression. GAPDH (forward 5′-ACCACAGTCCATGCCATCAC-3′ and reverse 5′-CACCACCCTGT TGCTGTAGCC-3′) was used as housekeeping gene.

Immunoblot analysis

m5S cells (4×10^4 cells per ml) were cultured in 6 well culture dish and incubated with various doses of Au^{Qur}NP (0, 0.5, 1.0, 5.0 and 10 µg l^{-1}) or pure quercetin (15 ng ml^{-1}) for 4 h. Treated cells were washed with cold PBS and lysed using RIPA buffer (20 mM Tris–HCl (pH 7.5), 150 mM NaCl, 1 mM Na$_2$EDTA 1 mM EGTA, 1% NP-40, 1% sodium deoxycholate, 2.5 mM sodium pyrophosphate 1 mM β-glycerophosphate, 1 mM Na$_3$VO$_4$) with 0.5% protease cocktail (Nacalai, Tesque, Inc, Tokyo, Japan). Protein samples were resolved over 10% SDS-PAGE gels and electroblotted onto PVDF membrane using Trans-Blot SD semi dry transfer cell (BioRad laboratories, CA, USA). Membranes were blocked with 5% (w/v) fetal bovine serum albumin and incubated overnight with specific primary antibodies; rabbit monoclonal antibodies for SMAD 2–4 (Cell signaling Technologies, MO, USA); mouse monoclonal antibody for TGFβ1

(Abcam Ltd, Cambridge, UK). Rabbit monoclonal antibody for β actin (Cell signaling technology, MO, USA) was used as loading control. After standard procedures of washing, membranes were incubated with HRP-conjugated anti-rabbit antibody for SMAD 2–4 (Cell signaling technology, MO, USA), and HRP-conjugated anti-mouse antibody for TGFβ1 for 1 h at room temperature. Expression of proteins was detected by chemiluminescence using ECL Plus western blotting detection system (Amersham Life Science, Inc., Buckinghamshire, UK). The intensities of the protein bands were quantified with the digital imaging system (LAS 4000, Fujifilm, Tokyo, Japan) and images were quantified using band intensities by using Image Quant TL Software (GE Healthcare, Tokyo, Japan).

Immunofluorescence studies

m5S cells were cultured on culture compatible gelatin (0.1%) coated cover slips and incubated with 5 µg l^{-1} AuNP or Au^{Qur}NP for 4 h. Cells were fixed in 4% PFA, permeabilized with 0.1% Triton-X, and blocked with 5% BSA, using Image-IT Fix-Perm Kit (Thermo-Fisher Scientific, MA, USA). The coverslips were incubated with rabbit monoclonal antibodies for SMAD 2, 3 or SMAD 4 (Cell signaling Technologies, MO. USA) at 4 °C overnight. Cells were subsequently washed in washing buffer and incubated with Alexa-Fluor-488 conjugated goat anti-rabbit IgG secondary antibodies (Thermo-Fisher Scientific, MA, USA). Nuclei were stained with 4′,6-diaminido-2-phenylindole (DAPI), and coverslips were mounted in Perma-Fluor mounting media (Thermo-Fisher Scientific, MA, USA). Images were captured under oil immersion (65× magnification) by using confocal microscope (TCS SP8, Leica, Wetzler, Germany).

In vitro cell migration assay

In vitro wound healing assay was performed using m5S fibroblast and PHK 16-0b human keratinocytes grown in µ-dish culture inserts (Ibidi Suppliers, Lochhamer, Grafelfing, Germany). Cells were cultured in culture vessel supported with µ-dish culture insert to confluency. During the confluent stage, culture inserts were slowly removed without disturbing the edge, to mimic the wound. Cells were treated with or without 5 µg l^{-1} AuNP, Au^{Qur}NP and quercetin (15 ng ml^{-1}) and photographed at various time laps periods (0, 4, 8, 16, 24 h). Rate of cell migration (mm) in various groups was calculated by using Image J software (NIH, Washington, USA). Live cell migration of keratinocytes was recorded by time lapse video device (Cyto smart-II, Lonza, Inc., Morristown, NJ, USA). Untreated cells were considered as control group.

Statistical analysis

All experiments were performed in triplicate with three independent experiments. Data is expressed as mean ± standard deviation. Mean differences between the groups were analyzed by two-way ANOVA with *post hoc* Dunnett's test with significant values of $p < 0.05\%$, $p < 0.01\%$.

Results and discussion

Major challenges in wound healing include drug efficiency, inefficient delivery, and wound edge cell oxidation stress phenomenon. Currently, there is a pressing need for nano-formulation based conjugates with multi-modal actions. Earlier, we reported the synthesis of Au^{Qur}NPs and its biosafety aspects on skin fibroblasts.[24] Quercetin up to 527 μM is safe for use in biomedical applications.[27] Quercetin is a proven dietary supplement with anti-oxidant property; its bioavailability and therapeutic action is mainly focused on cancer prevention. In the human body, it interacts with tissues such as small intestine, pancreas, skeletal muscle and liver to control body glucose haemostasis and other chronic diseases mostly by anti-oxidant mechanism.[28] In this study, we elucidated it effect on fibroblasts and keratinocyte cell migration in wound healing scenario. Polyphenols like quercetin, curcumin, and catechins are considered as sources of reducing cum stabilizing agents for preparation of metal nanoparticles, especially Ag and Au.[29] We used Flex X based bioinformatics to predict the interaction and bonding angle between Au metal and quercetin. The active site was found to be comprised of Au atoms (Fig. 1A). The execution of docking resulted in the interaction between hydroxyl and

Table 1 Mean size and standard deviation obtained by samples of AuNP and Au^{Qur}NP

	Mean size (nm)	Mean width (nm)
AuNP	27.45 (±3.6)	18 (±1.8)
Au^{Qur}NP	39.58 (±716)	22 (±4.9)

carbonyl groups of quercetin with Au atoms. Based on the model obtained, we opine that quercetin effectively reduced AuCl$_4$ to Au, resulting in formation of Au^{Qur}NP through energy balance reaction. However, further chemo-biological studies with more precise analyses are necessary to validate the energy balance mechanism between Au and quercetin. The conjugation between Au and quercetin was further authenticated by TEM analysis, which revealed uniform shape (mostly spherical) and an increase in the size of Au^{Qur}NPs in comparison to stand alone AuNPs (Fig. 1B). The amount of free quercetin varied from 3.8 (±1.5) to 5.2 (±1.6) in Au^{Qur}NP material (ESI Table 1†) as revealed by quercetin entrapment study. In order to check the intensity size distribution of AuNP and Au^{Qur}NP colloidal
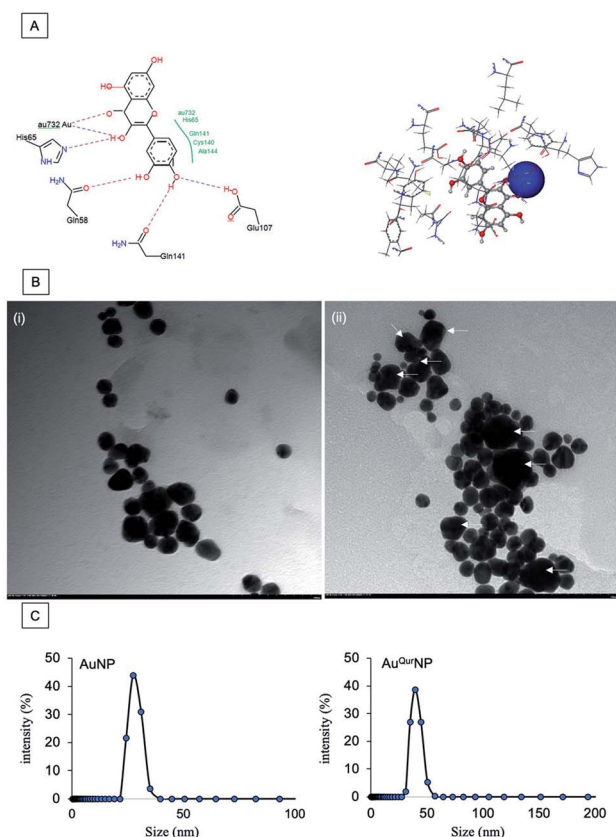

Fig. 1 (A) Bioinformatic analysis of AuNP with quercetin moiety by Flex X software. (B) Surface morphometry analysis by TEM to show the shape and morphology of (i) AuNP and (ii) Au^{Qur}NP. White arrow indicates the size increased NP. (C) Particle size *vs.* intensity (%) analysis determination by DLS method.
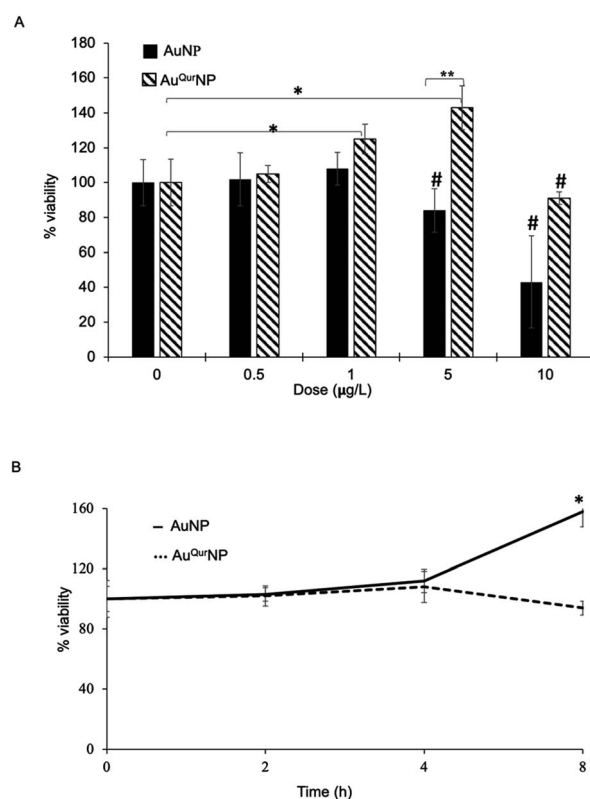

Fig. 2 MTT based cell viability and cell proliferation assay of fibroblast. (A) Cells were treated with AuNP or Au^{Qur}NP (0, 0.5, 1, 5 and 10 μg l^{-1}) and total viable cells were analyzed and represented as percentage of viable cells. (B) Cell proliferation assay. AuNP (5 μg l^{-1}) and Au^{Qur}NP (5 μg l^{-1}) were used at various time period and represented as percentage of viable cells. All experiments were conducted at least 3 times with independent groups. $p < 0.01\%$ *versus* control. *$p < 0.05\%$ *versus* control. #$p < 0.01\%$ *versus* control. **$p < 0.05\%$ between group.
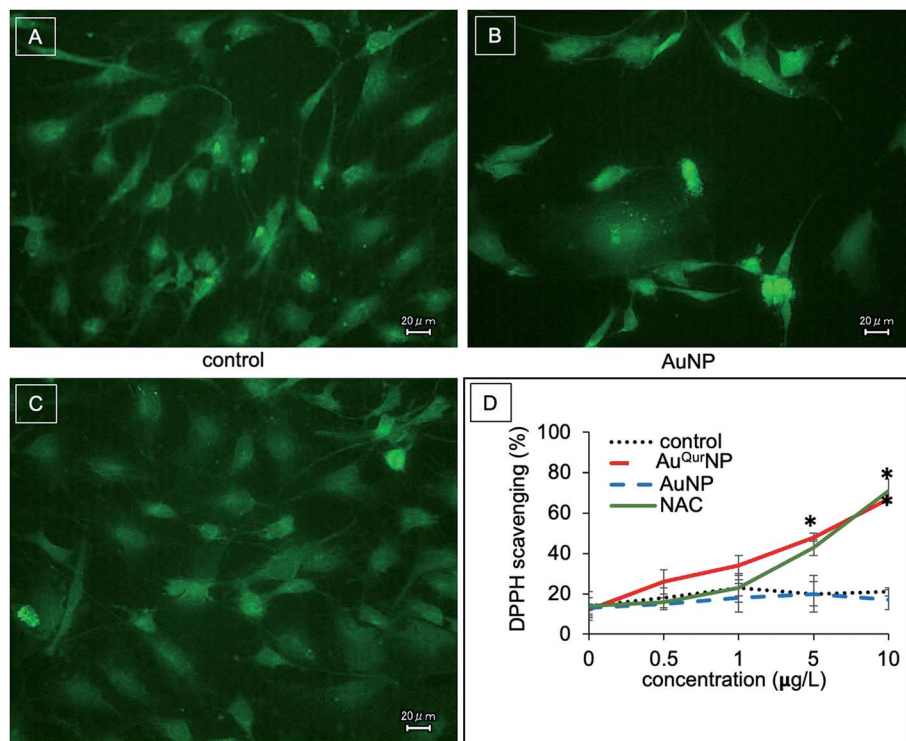
Fig. 3 ROS analysis by DCFH-DA fluorescence assay. (A) Untreated group. (B) AuNP (5 μg l^{-1}) treated group. (C) Au^{Qur}NP (5 μg l^{-1}) group. Intensity of green fluorescence indicates the degree of ROS production. (D) *In vitro* radical scavenging activity of AuNP, Au^{Qur}NP and positive control *NAC* at various dose (0, 0.5, 1.0, 5.0, and 10.0 μg l^{-1}). *$p < 0.05\%$ versus* control.
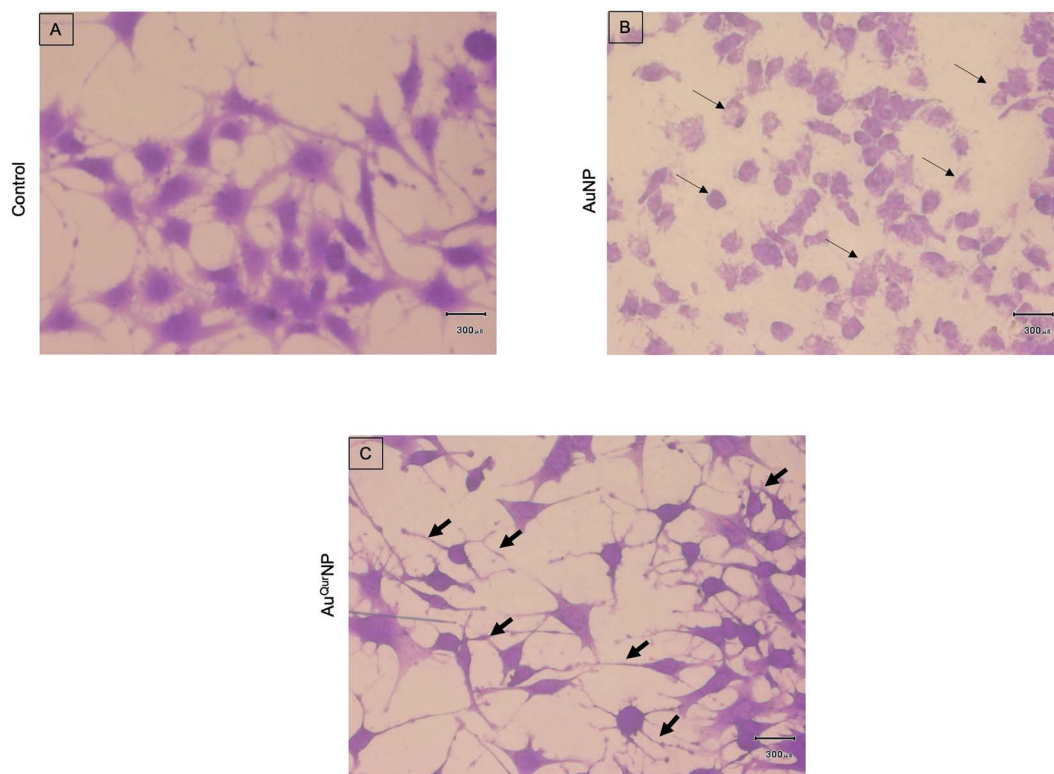

Fig. 4 Cell morphology changes during NPs treatment. (A) Untreated control group. (B) AuNP (5 μg l^{-1}) treated group. (C) Au^{Qur}NP (5 μg l^{-1}) stimulated group. Black thin arrow indicates the cell shrinkage during AuNP (5 μg l^{-1}) treatment, black thick arrow indicates regenerated fibril after treatment with Au^{Qur}NP. Photographs were taken at 40× magnification in bright field microscope. Scale bar 300 μm.
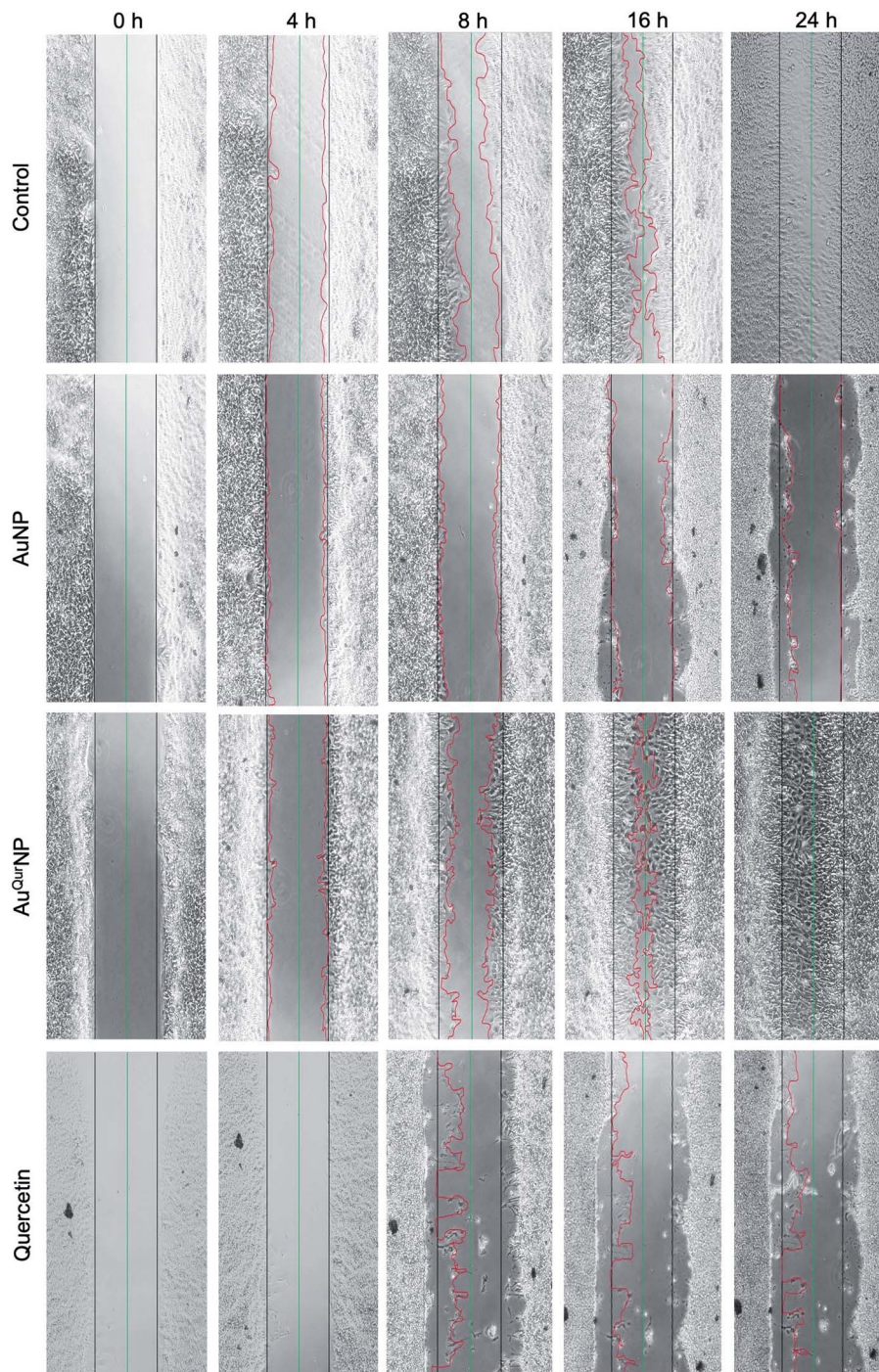
Fig. 5 *In vitro* wound healing assay. m5S fibroblasts were cultured in Ibidi culture insert. Confluent cells were treated with AuNP (5 μg l⁻¹) or Au^Qur^NP (5 μg l⁻¹) or pure quercetin (15 ng ml⁻¹) for different time period (0, 4, 8, 16, and 24 h). Non treated cells were used as control. Black line; starting point of cell migration. Green line; end point of cell migration. Red line; migratory cell edge. Photographs were taken in bright field microscope with magnification of 20×.

system, we performed the regularisation algorithm pattern by DLS method and presented the data in frequency curve mode (Fig. 1C). A slight increase in mean size (39.58 nm) and width (22 nm) of the Au^{Qur}NP from that of AuNP (27.45 ± 3.6 nm) and width (18 ± 1.8 nm) was noticed (Table 1). It is believed that incorporation of quercetin into NPs may cause hydrophobic interactions between the particles, resulting in surface func-tionalisation and increased size of NPs. Present study confirmed the earlier report of surface interaction phenomenon.[13]

We next proceeded to evaluate the bio-efficacy of AuNP and Au^{Qur}NPs, using mouse skin fibroblast cells. Fig. 2 shows the
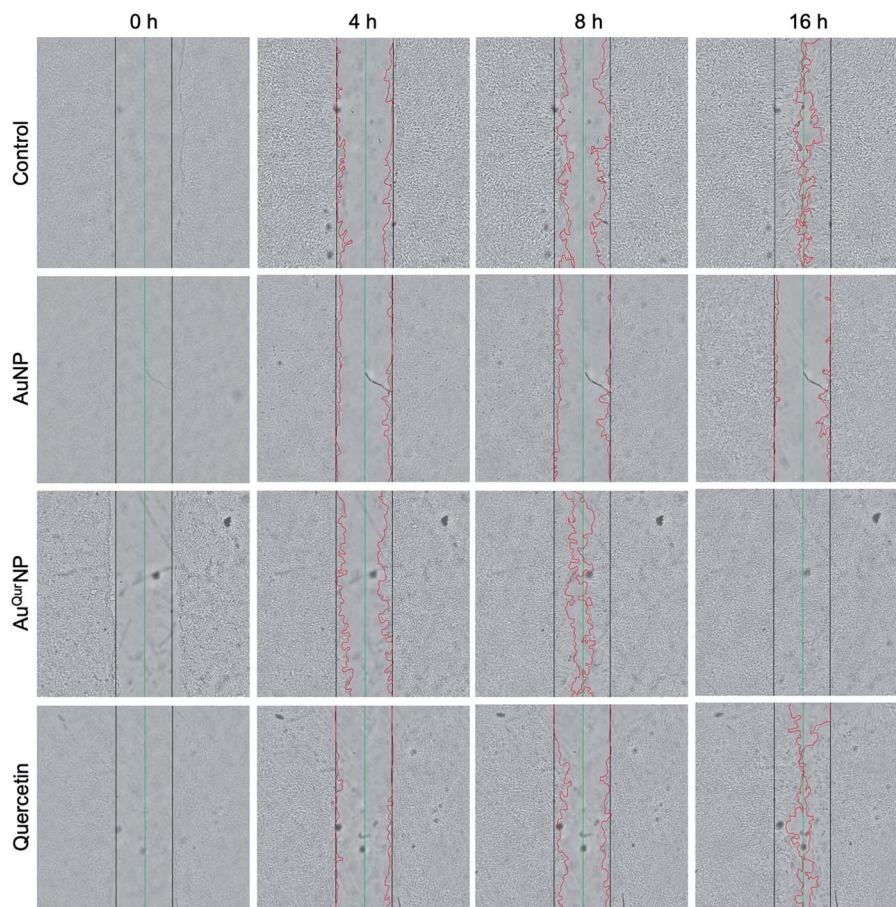
Fig. 6 *In vitro* wound assay. Human keratinocyte cells were cultured in Ibidi culture insert up to confluent stage. Cells were treated with AuNP (5 µg l^{-1}) or Au^{Qur}NP (5 µg l^{-1}) or pure quercetin (15 ng ml^{-1}) for different time period (0, 4, 8, 16 h). Non treated cells were used as control. Black line; starting point of cell migration. Green line; end point of cell migration. Red line; migratory cell edge. Photographs were taken in bright field microscope with magnification of 10×.

dose- and time-dependent effects of AuNP and Au^{Qur}NPs on cell viability and proliferation. Cells were treated with different doses of AuNP and Au^{Qur}NPs for 16 h and subjected to MTT assay. Au^{Qur}NPs up to a concentration of 5 µg l^{-1} was not cytotoxic (Fig. 2A). Rather, a dose- and time-dependent increase (Fig. 2B) in the number of viable cells was observed, with maximal effect obtained with 5 µg l^{-1} at 8 h. Interestingly, AuNPs at the same concentration caused a 20% reduction in viable cells compared to control cells. There are reports on cytotoxicity of NPs, mainly mediated by oxidative stress.[30] The presence of quercetin erased out the cytotoxic effect of AuNPs. These results indicate that Au^{Qur}NPs served the twin purpose of preventing cell death and simultaneously, enhancing proliferation of fibroblasts. External stimulation by nanomaterial leads to disturbances in mammalian cell membrane and leads to ROS generation.[31] In the present investigation, AuNP induced the generation of ROS in fibroblasts but Au^{Qur}NP attenuated the Au-induced intracellular ROS generation (Fig. 3). Quercetin is a known anti-oxidant nutraceutical and is used as adjuvant biomaterial in many regenerative research arena.[32] Free radical DPPH scavenging assay revealed that quercetin's anti-oxidant property was preserved in the Au^{Qur}NPs. AuNP alone was not

effective in scavenging the free radicals, but Au^{Qur}NPs exhibited high anti-oxidant activity and degree of radical scavenging activity was on par with *N*-acetyl cysteine (Fig. 3D). It is evident from these accumulated results that free radical scavenging mechanism of quercetin played a significant role in protecting the cells from Au-induced oxidative stress (Fig. 3C). It is universally accepted that stimulation of cells with NPs can result in morphological changes due to nano-biointerface, surface functionalization, shape, type and size of the NPs.[33] We observed condensed nucleus and reduced spindle formations in AuNP treated cells (Fig. 4), indicating damage to fibrils. In comparison, Au^{Qur}NP treated cells (Fig. 4C) exhibited elongated fibrils, depicting enhanced fibrilogenesis probably due to more collagen synthesis. The protective effect of Au^{Qur}NPs in maintaining cell shape and structure provides evidence that anti-oxidant functionalized NPs have a protective role in cell physiology and function. It is quite evident that AuNP is causing stress to the cell, characterized by nuclear condensation and shortening of the fibrils (Fig. 4B). However, stress phenomenon was abolished with Au^{Qur}NP treatment, confirming the beneficiary action of quercetin. From the results of toxicity end point assay (Fig. 2), ROS stress and radical scavenging assay (Fig. 3)
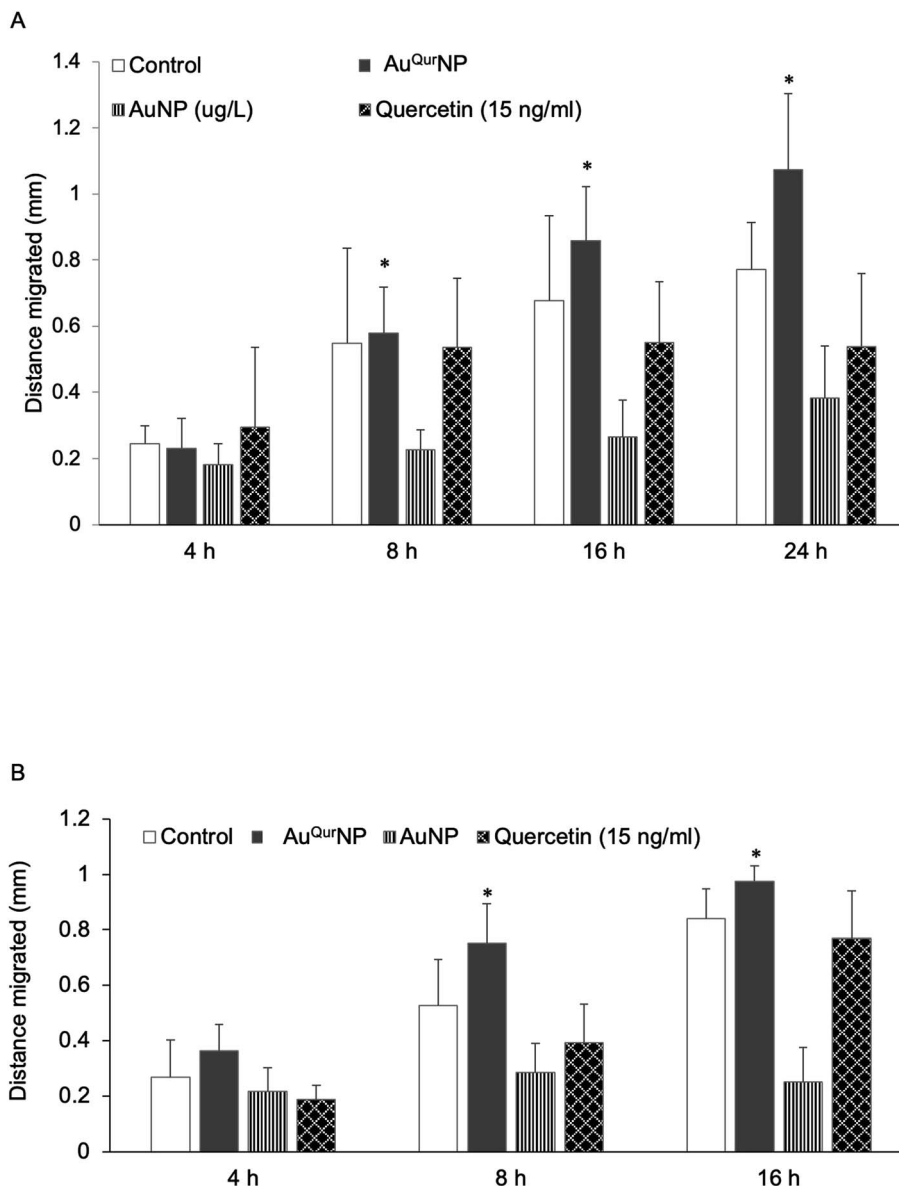
Fig. 7 Quantification of cell migration. (A) Degree of fibroblast cell migration were quantified after treatment with AuNP (5 µg l^{-1}) or Au^{Qur}NP (5 µg l^{-1}) or pure quercetin (15 ng ml^{-1}) at different time intervals of 4, 8, 16 and 24 h. Untreated cells were considered as control. (B) Graphical representation of keratinocyte cell migration treated with AuNP (5 µg l^{-1}) or Au^{Qur}NP (5 µg l^{-1}) or pure quercetin (15 ng ml^{-1}) at different time intervals of 4, 8, and 16 h. Untreated cells were considered as control. Distance migrated by the cells were calculated in mean millimeter distance from edge using Image-J software.

and cell morphometry analysis (Fig. 4), it is clear that AuNP and Au^{Qur}NP displayed opposite effects on the fibroblasts. This phenomenon of stress prevention is explained by cellular adaptive nature to gold NPs provided with suitable surface coating, shape, size, and duration of the exposure. Similar phenomenon was observed by another study which showed that, surface chemistry of gold NPs plays a determining factor in cell stress.[34] Therefore, we proceeded to identify the molecular interaction of Au^{Qur}NP with the cells. The process of fibrilogenesis controls the movement and migration of skin fibroblasts, a hallmark of many physiological events, including

wound healing.[24,35] Studies show that free radical scavenging agents can accelerate the rate of healing of wounds.[13,36] To test if Au^{Qur}NPs could be stimulating cell migration, we monitored the movement of Au^{Qur}NP treated cells by standard *in vitro* scratch assay that simulates wound healing. Eight hours treatment with Au^{Qur}NPs resulted in significant increase in the migration of fibroblasts, as is evident in Fig. 5. Keratinocytes showed complete migration in 16 h (Fig. 6). The migratory potential of fibroblasts and keratinocytes is shown in Fig. 7. In 24 h duration, AuNP (5 µg l^{-1}) treated fibroblasts did not show any significant migration, while, Au^{Qur}NP (5 µg l^{-1} with free
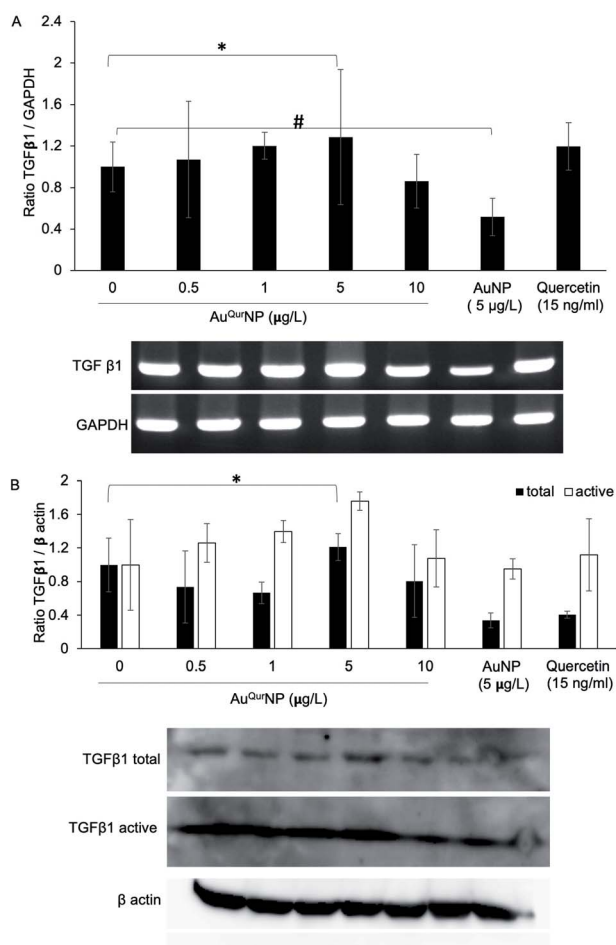
Fig. 8 Semi quantitative reverse transcription–polymerase chain reaction and western blot analysis. (A) mRNA expression of TGFβ1 after 4 h treatment with Au^{Qur}NP (0, 0.5, 1, 5 and 10 µg l^{-1}). (B) Western blot results of TGFβ1 (total as well as active) upon Au^{Qur}NP treatment (0, 0.5, 1, 5 and 10 µg l^{-1}) for 4 h. AuNP (5 µg l^{-1}) and quercetin (15 ng ml^{-1}) were used as parallel controls. Readings are average of three independent experiments. *$p < 0.05\%$ versus control. #$p < 0.01\%$ versus control.

Fig. 9 Western blot analysis of SMAD proteins (SMAD 2, 3, 4, and 7), upon treatment with Au^{Qur}NP for 4 h. AuNP (5 µg l^{-1}) and quercetin (15 ng ml^{-1}) were used as parallel controls. Readings are average of three independent experiments. *$p < 0.05\%$ versus control. #$p < 0.01\%$ versus control.

quercetin of 4.6 ± 0.6) significantly ($p < 0.5\%$) induced 1.03 mm of migration than any other group (Fig. 7A). Keratinocytes displayed faster migration than the fibroblasts in terms of time taken to migrate (Fig. 7B). The degree of migration of fibroblasts and keratinocytes was in the order of Au^{Qur}NP > control > quercetin > AuNP. The promotive role of quercetin in wound healing scenario is well documented[37] and has been successfully used as a component of scaffolds and hydrogel based wound dressings.[36,38,39] The specific mechanisms by which quercetin NPs enhance healing of wounds is not yet elucidated. It is probable that Au^{Qur}NP functions through inducing collagen synthesis[24] and elongated fibrilogenesis (Fig. 4C). We also confirmed that Au^{Qur}NP treatment cumulatively helped in the migration of keratinocytes which is quite evident from live cell migration data (ESI Video†).

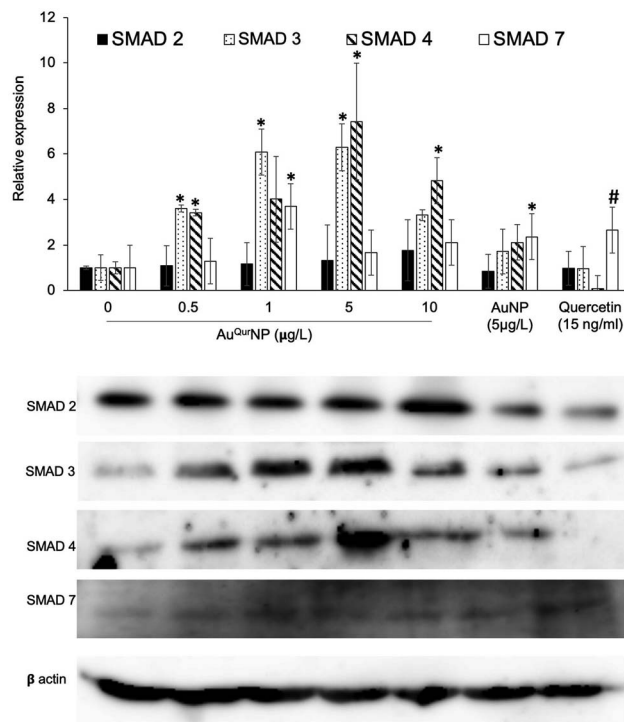Wound healing is a complex phenomenon, involving timely co-ordination between the phases of inflammation, cellular proliferation cum migration, and tissue remodelling. The growth factor TGFβ1 plays a prominent role in all aspects of the healing process, through regulating the expression of key components necessary for healing, such as ECM proteins, angiogenic factors, and proteins that facilitate proliferation and migration of cells.[40] In addition, TGFβ1 is major signalling junction of fibrosis and scar formation during the later phase of wound healing through its direct target on several genes. The direct link between TGFβ1 dynamics and formation of secondary DNA structures like guanine rich quadruplexes in fibroblast cell during skin scar formation are well documented.[41] Effective wound scar management and suitable alternate therapy by engineered scaffold encapsulated antiscaring agent like PXS64, a neutral analogue of mannose-6-phosphate has been developed to inhibit the activation of TGFβ1.[42] The mechanism of action of PXS64 is by selectively targeting the mannose-6-receptor.[43] Since Au^{Qur}NP was observed to spike an increase in both proliferation and migration of cells, we asked if TGFβ1 was involved in the phenomenon. PCR analysis did not reveal any significant increase in TGFβ1 at the mRNA level (Fig. 8A). However, Au^{Qur}NPs treatment induced a significant increase in the protein levels of TGFβ1 (Fig. 8B). It is clear that over activation of TGFβ1 with concomitant collagen production may lead to scar formation in hyper activated fibroblast keloid cell. However, in the present investigation we used normal fibroblasts. Intrinsic molecular
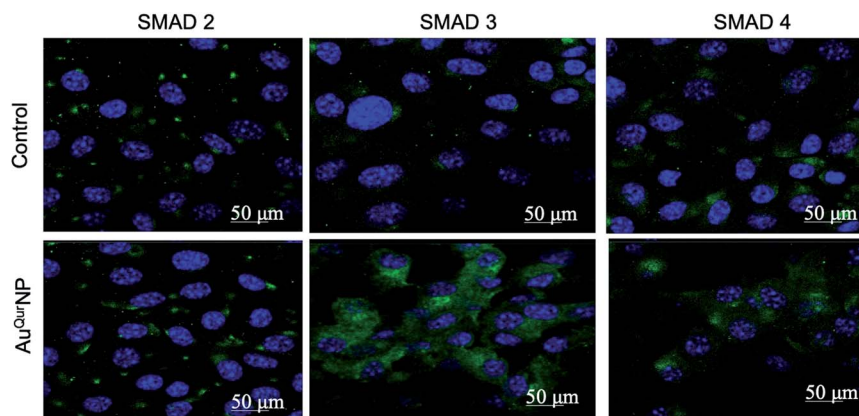
Fig. 10 SMAD nuclear translocation study. Immuno–cytochemistry experiments during Au^{Qur}NP (5 µg l^{-1}) treatment of fibroblast cells. Untreated cells served as control groups. Cells were probed with primary rabbit antibodies specific for SMAD 2, 3, or 4, followed by Alexa-488 conjugated anti-rabbit IgG antibodies. DAPI was used as nuclear staining probe. Fluoroscence photomicrographs were taken at 65× magnification.

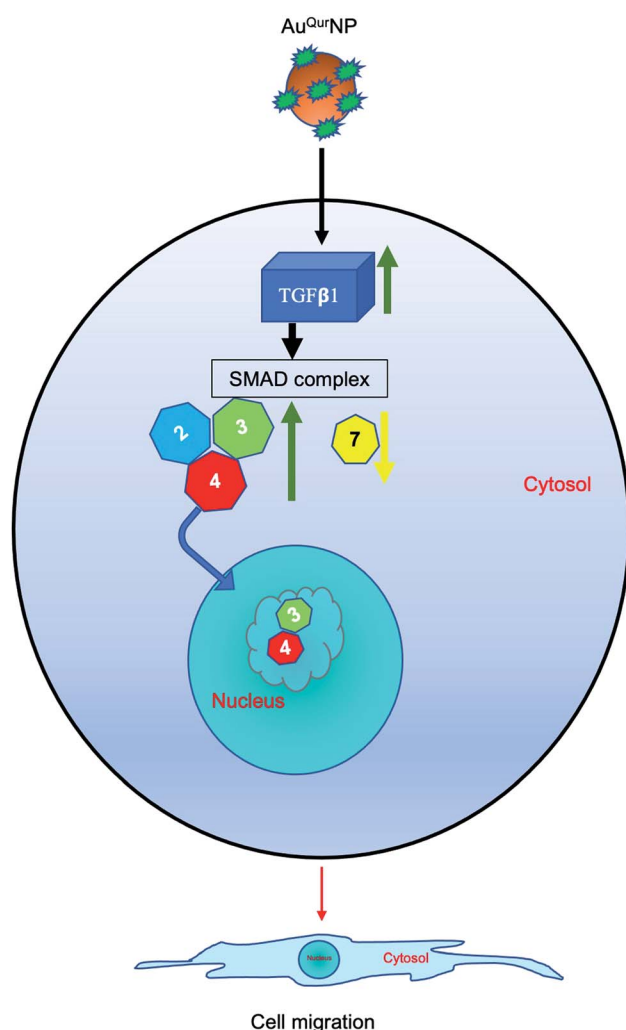**Fig. 11** Graphical conclusion. During Au^{Qur}NP stimulation to cell, SMAD complex (2–4) was over expressed and translocated to nucleus due to negative regulation of SMAD 7. This cumulatively assist to cell migration and probably helps in wound healing.

events in other fibroblast cells like keloid needs to be further investigated. TGFβ1 largely elicits its cellular functions through the canonical pathway involving activation of receptor SMADs (SMAD 2 and 3) and co-activator SMAD 4.[44] Treatment of cells with Au^{Qur}NP caused an increase in the expressions of SMADs 2–4, and a decrease in SMAD 7 (Fig. 9). SMAD 7 is an inhibitory SMAD that competes with the R-SMADs, preventing their activation and nuclear translocation.[44] Immunofluorescence studies confirmed that Au^{Qur}NPs induced the nuclear translocation of SMADs 3 and 4 (Fig. 10). Cells treated with quercetin displayed opposite results with reduction in expression levels of TGFβ1, and SMADs 2–4. Quercetin was reported to suppress the activation of SMADs in keloid fibroblasts.[45] It is probable that coupling of quercetin with Au helped the cells to escape from the negative regulation of TGFβ1 induced by quercetin. TGFβ1 and SMAD-signalling cascade have intricate actions during fibroblast migration in wound healing.[16,46] The opposite action of native quercetin and Au^{Qur}NP towards the cell can be explained by absorption kinetics and bioavailability of trapped quercetin material.[47] Our data is consistent with earlier report of accelerated wound healing by quercetin loaded chitosan NPs through TGFβ1-dependent mechanism,[48] and we believe it can be used as topical agent for dermal wound healing.

Conclusions

Fig. 11 depicts the whole mechanism in a nut shell. The current study examined the effect of colloidal AuNP coupled with quercetin on fibroblast cell migration assisted-wound healing mechanism. Au^{Qur}NPs showed beneficial effect on cell proliferation and migration of fibroblasts. Cell migration action of Au^{Qur}NPs was routed through the TGFβ1 dependent SMAD signaling pathway. Although more in-depth studies elucidating the molecular mechanisms involved need to be investigated, this preliminary study brings forth molecular cell biology evidence-based data to elevate the promising therapeutic applications of nanocuetical engineered gold particles in future nanomedicine for skin etiology.

Abbreviations

NP	Nanoparticle
AuNP	Gold nanoparticle
$Au^{Qur}NP$	Quercetin functionalized gold nanoparticle
DMSO	Dimethyl sulfoxide
DPPH	2,2-Diphenyl-1-picrylhydrazyl
DLS	Dynamic light scattering
NAC	N-Acetyl cysteine
DLS	Dynamic light scattering
ROS	Reactive oxygen species

Conflicts of interest

No potential conflict of interest was reported by the authors.

Acknowledgements

References

1 S. A. kumar and M. Harishkumar, in *Integrating biologically-inspired nanotechnology into medical practice*, ed. N. B. Kumar, N. Amin and B. A. Amin, IGI-Global, Hershey PA 17033, USA, 3rd edn, 2017, ch. 2, pp. 32–49.

2 S. Shankar, S. K. Soni, H. K. Daima, P. R. Selvakannan, J. M. Khire, S. K. Bhargava and V. Bansal, *Phys. Chem. Chem. Phys.*, 2015, **17**, 21517–21524.

3 E. Sánchez-López, D. Gomes, G. Esteruelas, L. Bonilla, A. L. Lopez-Machado, R. Galindo, A. Cano, M. Espina, M. Ettcheto, A. Camins, A. M. Silva, A. Durazzo, A. Santini, M. L. Garcia and E. B. Souto, *Nanomaterials*, 2020, **10**(2), 292–330.

4 P. Slepička, N. Slepičková Kasálková, J. Siegel, Z. Kolská and V. Švorčík, *Materials*, 2019, **13**(1), 1–22.

5 W. M. Dabeek and M. V. Marra, *Nutrients*, 2019, **11**(10), 2288–2306.

6 A. Massi, O. Bortolini, D. Ragno, T. Bernardi, G. Sacchetti, M. Tacchini and C. De Risi, *Molecules*, 2017, **22**(8), 1270–1297.

7 R. Ghafelehbashi, M. Tavakkoli Yaraki, L. Heidarpoor Saremi, A. Lajevardi, M. Haratian, B. Astinchap, A. M. Rashidi and R. Moradian, *Mater. Sci. Eng., C*, 2020, **109**, 110597.

8 S. Naqvi, H. Sharma and S. J. Flora, *Int. J. Nanomed.*, 2019, **14**, 8943–8959.

9 S. T. Shah, W. A. Yehye, Z. Z. Chowdhury and K. Simarani, *PeerJ*, 2019, **7**, e7651.

10 O. Lozano, A. Lázaro-Alfaro, C. Silva-Platas, Y. Oropeza-Almazán, A. Torres-Quintanilla, J. Bernal-Ramírez, H. Alves-Figueiredo and G. García-Rivas, *Oxid. Med. Cell. Longevity*, 2019, **2019**, 7683051.

11 P. N. Navya, A. Kaphle, S. P. Srinivas, S. K. Bhargava, V. M. Rotello and H. K. Daima, *Nano Convergence*, 2019, **6**, 23.

12 I. Castangia, A. Nácher, C. Caddeo, D. Valenti, A. M. Fadda, O. Díez-Sales, A. Ruiz-Saurí and M. Manconi, *Acta Biomater.*, 2014, **10**, 1292–1300.

13 G. H. Lee, S. J. Lee, S. W. Jeong, H. C. Kim, G. Y. Park, S. G. Lee and J. H. Choi, *Colloids Surf., B*, 2016, **143**, 511–517.

14 F. Mansourizadeh, D. Alberti, V. Bitonto, M. Tripepi, H. Sepehri, S. Khoee and S. Geninatti Crich, *Colloids Surf., B*, 2020, **191**, 110982.

15 D. George, P. U. Maheswari and K. M. M. S. Begum, *Carbohydr. Polym.*, 2020, **236**, 116101.

16 J. P. Jee, R. Pangeni, S. K. Jha, Y. Byun and J. W. Park, *Int. J. Nanomed.*, 2019, **14**, 5449–5475.

17 M. S. Abate, L. R. Battle, A. N. Emerson, J. M. Gardner and S. C. Shalin, *Arch. Pathol. Lab. Med.*, 2019, **143**, 919–942.

18 H. Madhyastha, R. Madhyastha, Y. Nakajima, S. Omura and M. Maruyama, *Clin. Exp. Pharmacol. Physiol.*, 2012, **39**, 13–19.

19 H. K. Madhyastha, K. S. Radha, Y. Nakajima, S. Omura and M. Maruyama, *J. Cell. Mol. Med.*, 2008, **12**, 2691–2703.

20 R. Madhyastha, H. Madhyastha, Y. Nakajima, S. Omura and M. Maruyama, *Int. Wound J.*, 2012, **9**, 355–361.

21 R. Madhyastha, H. Madhyastha, Y. Pengjam, Y. Nakajima, S. Omura and M. Maruyama, *Biochem. Biophys. Res. Commun.*, 2014, **451**, 615–621.

22 B. Blanco-Fernandez, O. Castaño, M. A. Mateos-Timoneda, E. Engel and S. Perez Amodio, *Adv. Wound Care*, 2020, **10**, 1089–1094.

23 M. L. de Souza, W. M. Dos Santos, A. L. M. D. de Sousa, V. de Albuquerque Wanderley Sales, F. P. Nóbrega, M. V. G. de Oliveira and P. J. R. Neto, *Curr. Pharm. Des.*, 2020, **26**(36), 4536–4550.

24 U. Medha, S. Sanjana, J. Devendra, M. Harishkumar, M. Radha, M. Masugi, N. Paduvarahalli and D. Hemantkumar, *Colloids Surf., A*, 2018, **548**, 1–9.

25 A. Steffen, A. Kämper and T. Lengauer, *J. Chem. Inf. Model.*, 2006, **46**, 1695–1703.

26 T. Mosmann, *J. Immunol. Methods*, 1983, **65**, 55–63.

27 J. Waizenegger, D. Lenze, C. Luckert, A. Seidel, A. Lampen and S. Hessel, *Mol. Nutr. Food Res.*, 2015, **59**, 1117–1129.

28 A. W. Boots, G. R. Haenen and A. Bast, *Eur. J. Pharmacol.*, 2008, **585**, 325–337.

29 F. Caputo, M. De Nicola and L. Ghibelli, *Biochem. Pharmacol.*, 2014, **92**, 112–130.

30 M. Harishkumar, M. Radha, N. Yuchi, D. H. Kumar, N. Paduvarahalli and M. Masugi, *Mater. Today: Proc.*, 2019, **10**, 100–105.

31 H. Madhyastha, R. Madhyastha, A. Thakur, S. Kentaro, A. Dev, S. Singh, B. Chandrashekharappa R, H. Kumar, O. Acevedo, Y. Nakajima, H. K. Daima, A. Aradhya, N. Nagaraj P and M. Maruyama, *Colloids Surf., B*, 2020, **194**, 111211.

32 W. Bors, C. Michel and M. Saran, *Methods Enzymol.*, 1994, **234**, 420–429.

33 N. Campolo, S. Bartesaghi and R. Radi, *Redox Rep.*, 2014, **19**, 221–231.

34 P. Falagan-Lotsch, E. M. Grzincic and C. J. Murphy, *Proc. Natl. Acad. Sci. U. S. A.*, 2016, **113**, 13318–13323.

35 F. Fernandez-Madrid, S. Noonan and J. Riddle, *J. Anat.*, 1981, **132**, 157–166.

36 T. Hatahet, M. Morille, A. Hommoss, J. M. Devoisselle, R. H. Müller and S. Bégu, *Eur. J. Pharm. Biopharm.*, 2016, **108**, 41–53.

37 A. Gopalakrishnan, M. Ram, S. Kumawat, S. Tandan and D. Kumar, *Indian J. Exp. Biol.*, 2016, **54**, 187–195.

38 I. Castangia, M. L. Manca, C. Caddeo, G. Bacchetta, R. Pons, D. Demurtas, O. Diez-Sales, A. M. Fadda and M. Manconi, *Eur. J. Pharm. Biopharm.*, 2016, **103**, 149–158.

39 W. S. Vedakumari, N. Ayaz, A. S. Karthick, R. Senthil and T. P. Sastry, *Eur. J. Pharm. Sci.*, 2017, **97**, 106–112.

40 M. Pakyari, A. Farrokhi, M. K. Maharlooei and A. Ghahary, *Adv. Wound Care*, 2013, **2**, 215–224.

41 P. Toshniwal, M. Nguyen, A. Guédin, H. Viola, D. Ho, Y. Kim, U. Bhatt, C. S. Bond, L. Hool, L. H. Hurley, J. L. Mergny, M. Fear, F. Wood, S. K. Iyer and N. M. Smith, *FEBS Lett.*, 2019, **593**, 3149–3161.

42 V. Agarwal, F. M. Wood, M. Fear and S. K. Iyer, *Aust. J. Chem.*, 2016, **70**, 280–285.

43 V. Agarwal, P. Toshniwal, N. E. Smith, N. M. Smith, B. Li, T. D. Clemons, L. T. Byrne, F. Kakulas, F. M. Wood, M. Fear, B. Corry and K. Swaminathan Iyer, *Chem. Commun.*, 2016, **52**, 327–330.

44 T. Ota, M. Fujii, T. Sugizaki, M. Ishii, K. Miyazawa, H. Aburatani and K. Miyazono, *J. Cell. Physiol.*, 2002, **193**, 299–318.

45 T. T. Phan, I. J. Lim, S. Y. Chan, E. K. Tan, S. T. Lee and M. T. Longaker, *J. Trauma*, 2004, **57**, 1032–1037.

46 A. Choudhary, V. Kant, B. L. Jangir and V. G. Joshi, *Eur. J. Pharmacol.*, 2020, **880**, 173172.

47 A. Vijayakumar, R. Baskaran, Y. S. Jang, S. H. Oh and B. K. Yoo, *AAPS PharmSciTech*, 2017, **18**, 875–883.

48 D. K. Chellappan, N. J. Yee, B. J. Kaur Ambar Jeet Singh, J. Panneerselvam, T. Madheswaran, J. Chellian, S. Satija, M. Mehta, M. Gulati, G. Gupta and K. Dua, *Ther. Delivery*, 2019, **10**, 281–293.